MEASUREMENTS ON A VERTICAL TAIL WITH VANE VORTEX GENERATORS

V. M. Singh, P. Scholz
Institute of Fluid Mechanics, TU Braunschweig, Braunschweig, D-38108, Germany

Abstract

This contribution presents the investigation of a passive method of boundary layer separation control on a swept and tapered vertical tail plane with a deflected rudder. The primary objective was the increase of the total side force coefficient. For that, an array of co-rotating vane vortex generators was placed close to the rudder knee to maintain an attached flow, which consequently led to an increase of the side force coefficient. The second objective was a parameter sensitivity study, which covered a large scope of different vane vortex generator parameters: size, shape, angle of attack, position and separation. Experiments were performed in a low-speed wind tunnel. The results show the ability of vane vortex generators to increase the side force coefficient for a large range of yaw angles. The maximal increase of side force coefficient was about 14 %. However, the influence of the vane vortex generators on the stall of the vertical tail plane was limited. Nevertheless, in a range of yaw angles, an increase of the lift to drag ratio of about 30 % was obtained. The effect was found to be sensitive for the angle of attack, chordwise position, size and geometry of a vortex generator, whereas parameters such as spanwise extension and separation were less sensitive to parameter change.

NOMENCLATURE

AoA	Angle of attack of a VVG
BL	Boundary layer
CFD	Computational fluid dynamics
IOE	One-engine inoperative
L/D	Lift to drag ratio
LE	Leading edge
Re	Reynolds number
SG	Strain gauge
SL	Separation line
TBL	Turbulent boundary layer
TE	Trailing edge
VG	Vortex generator
VVG	Vane vortex generator
b	VTP height; span, m
c	chord length, -
C_Y	Side force coefficient, -
C_W	Drag coefficient, -
n	amount of VVG, -
T	Temperature, °C
U_∞	Undisturbed inflow velocity, m/s
U_e	Velocity at the BL edge, m/s
α	AoA of a VVG, °
β	yaw angle, °
γ	local flow angle with respect to line of flight, °
δ	Boundary layer thickness, m
δ_r	rudder deflection angle, °
ε	angle of incidence of a VVG, °
η	dimensionless spanwise, -
λ	Taper ratio, -
λ_{VVG}	Aspect ratio of an VVG: $\lambda_{VVG} = l/h$, -
φ_{LE}	Leading edge sweep angle, °

1. INTRODUCTION

The main objective of vertical tail planes (VTP), as seen on modern transport aircrafts, is to ensure full stability and control over the aircraft during all flight phases and maneuvers. Although the main part of the mission profile is usually the cruise flight, it is not the critical design point for a VTP. Instead, the event of a one-sided engine failure during the take-off has major influence on the VTP design. During a one-engine inoperative (IOE) event, an asymmetric thrust distribution occurs that generates a yaw moment around the vertical axis. To maintain control over the aircraft, a stabilizing moment is required. According to certification rules, only rudder control alone must be sufficient to maintain the control over the aircraft [1]. Hence, during the critical event of an engine failure on the runway, the VTP alone must generate the necessary side force. However, as soon the aircraft is airborne, a bank angle is additionally applied with the help of the ailerons to keep the aircraft on its flightpath. Since the aircrafts velocity is relatively low during the take-off, the required side force for an IOE event is realized by enlarging the size of the VTP. Therefore, the size of the VTP is dominated by the IOE-event. Considering that the size of the VTP is determined by a rare event and the economical disadvantages, e.g. fuel consumption of an over-sized VTP, the optimization potential becomes clear. If the side force potential of the VTP could be increased, its size could be reduced. Hence, weight and drag could be reduced, which would consequently enhance fuel consumption.
Due to this potential, investigations of VTPs are of major interest. For example, Boeing and NASA showed successfully during flight tests the technical feasibility of active flow control on a VTP. Moreover, wind tunnel tests on a full scale 757 VTP showed an increase of the side force by 20 to 30 % using active flow control jets that were positioned close to the rudder knee. [2][3]

The primary objective of the study presented in this paper is the increase of the side force of the VTP at large rudder deflections, where flow on the rudder is completely detached. To suppress or at least delay flow separation on the rudder, a co-rotating array of vane vortex generators (VVGs) was mounted onto the surface of the suctions side

close to the rudder knee. These VVGs generate longitudinal vortices that mix the turbulent boundary layer (TBL) and therefore enhance the momentum exchange inside the BL. As a result, the TBL is less prone to adverse pressure gradients and separation can be delayed. The second objective of this study is to investigate parameters to determine their effect on the VTP's flow. Therefore, the size, shape, AoA, position and the separation of VVGs were varied.

The investigation of passive flow control methods has been subject of research for many years. An extensive overview of different fields of application of low-profile VGs, also known as micro VG, submerged VG or microvanes, is given in [4]. Low-profile VVGs are characterized by their height, which is between 10 % and 50 % of the BL thickness. According to [5], low-profile VGs have the potential of increasing the efficiency when generating a comparable effect as conventional VVGs with $h/\delta \approx 1$ while reducing drag. In [6], experiments on a two-dimensional backward facing ramp were conducted, which showed that the optimal height to BL thickness ratio is $h/\delta = 0.8$ for the counter rotating set up. The findings in [7], where a similar test case was investigated, concluded that the counter-rotating set up is 100 % more efficient than the co-rotating set up. Regarding the shape, results in [7] also show that triangular shaped VVGs of $h/\delta = 0.2$ are 20 % more efficient than square shaped VVGs of the same height. Further, it was pointed out that the optimal aspect ratio of an VVG is $\lambda = 2.5$ and should not be smaller than $\lambda = 2$. The optimal AoA of a VVG was found to be at $\alpha = 18°$.
However, those results have been generated in quasi two-dimensional experiments. It is yet unclear if 2D-results can simply be transferred to more complex problems. Three-dimensional investigations showed that the effectiveness of VGs is dependent on the rotational direction of the longitudinal vortex [8][9][10]. In [11], it was concluded that on a swept wing, the configuration with co-rotating longitudinal vortices are more efficient compared to the counter-rotating set up. 2.5D simulations of a swept wing with counter-rotating low profile VVG positioned on the upper part of the flap showed that a pair of VVGs generates different large longitudinal vortices [12]. It was pointed out that as long the local flow direction is unclear, a co-rotating set up perpendicular to the flap LE should be preferred over the counter-rotating orientation [12]. During the AWIATOR program, wind tunnel and flight tests were performed in which co-rotating low-profile VVGs were placed on the flap of an A340-300 wing. The result was that the flow separation on the flap was delayed and hence a higher deflection from 32° to 35° could be realized, which resulted in an increase in lift of 2.5% during landing [13].
Wind tunnel experiments conducted on a highly swept wing of finite span with a drooped LE and TE showed that VVGs in a co-rotating array delayed the trailing edge separation. As a result, the lift dependent drag was reduced by 10 %. Moreover, a parameter variation of the chordwise position and the AoA of VVGs were investigated. It was found that the chordwise position of the VVGs appears not that critical, as long the VVG height is of similar magnitude as the BL thickness. Additionally, a VVG height to BL thickness ratio of $h/\delta \approx 1$ was recommended and an AoA between $18° < \alpha < 23°$ of the VVG with respect to the local flow direction was suggested as a desirable setting. However, during the parameter study the most effective configurations were measured for the range of $18° < \alpha < 30°$. [14]

Since this paper discusses a similar experimental setup, as shown in [14], these results will be used here primarily for the selection of suitable parameters. However, both models still differ in a various number of geometrical characteristics. With respect to the presented studies and results, the investigation of VVGs on a swept and tapered VTP with a deflected ruder is highly interesting, especially the investigation of a complete scope of parameters.

2. EXPERIMENTAL SETUP

2.1. Model

The wind tunnel model is based on the conventional tail configuration of modern transport aircrafts, in which the vertical tail is a swept wing of finite span with a symmetrical profile. FIG 1 shows the lateral view of the VTP model and its geometrical characteristics. The model consists of two parts, a fixed fin and a deflectable rudder. For the parameter study of the VVGs rudder deflections of $\delta_r = 15°, 30°, 35°$ were set. The span of the model is $b = 0.8502$ m and the taper ratio is about $\lambda = 0.4$. The leading edge is swept back with $\varphi_{LE} = 46°$. The reference chord length is $c_{ref} = 0.5285$ m.

To prevent laminar separation bubbles, a one-sided zigzag shaped and 90 µm thick transition strip was placed on the leading edge of the model, with the zigzag pattern pointed in the direction of the stagnation point. It was checked in a series of preparative runs with different transition fixing tapes and positions that this type of fixing has a suitable thickness and placement.

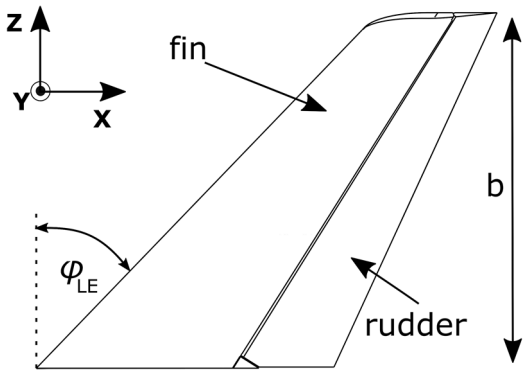

FIG 1: Sketch of the VTP model and its geometrical characteristics

2.2. Wind Tunnel

The experiments were conducted in the Modell-Unterschallkanal Braunschweig (MUB), a low speed closed return atmospheric wind tunnel. The test section has a cross section at the inlet of 1.3 m x 1.3 m and is 3 m long. To balance the increasing boundary layer thickness, the test sections floor and roof are inclined by 0.2°. The model was mounted onto a turning table in the test sections floor with a distance between the root leading edge of the model and the inlet of the test section of 1.15 m. The wind tunnel velocity was set to a constant free stream velocity of $U_\infty = 57$ m/s and temperature, which varied between $35°C < T < 40°C$. Thus, Reynolds numbers are in the range of $1.75 < Re < 1.80$ Million based on c_{ref}. The smallest Reynolds number at the tip of the model was 0.94 Million.

2.3. Vane Vortex Generator

The VVGs are made from 0.5 mm thick steel metal sheets. Each VVG is bended rectangular so that one side can be glued to the surface and the vortex generating part is orientated perpendicular to the surface of the VTP. FIG 2 shows the shapes and dimensions of the vortex generating part of the investigated VVGs.

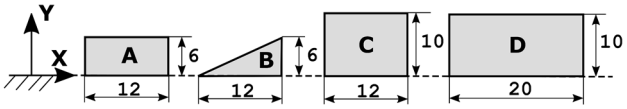

FIG 2: Overview of the investigated VVGs; dimensions in mm

During the parameter study, different positions of the VVGs were investigated. A summary of all selected positions on the VTP is given in FIG 3. Each configuration consists of an array of VVGs along the line of constant chord length $x/c = const.$ and an equal spacing between the VVGs $\Delta\,\eta = const.$

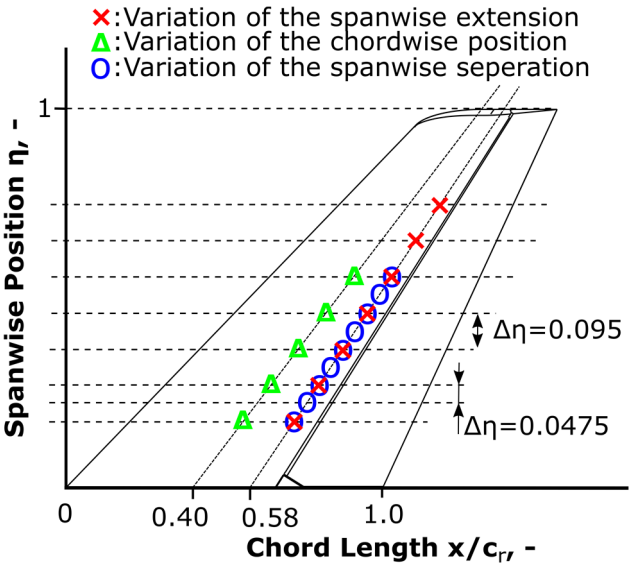

FIG 3: Positions of the VVGs on the surface of VTP

Since a three-dimensional BL occurs on swept wings, local flow properties at each VVG must be known. FIG 4 illustrates the flow situation at a VVG.

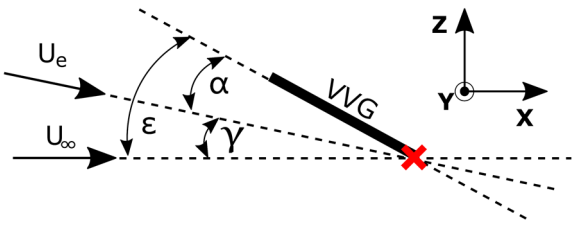

FIG 4: Schematic local angle definition for a single VVG

In this sketch, the local flow vector is represented by the velocity vector at the edge of the BL U_e. However, the local flow angle γ changes over the height of a VVG due to the twisted velocity profile of the BL. Therefore, the velocity profiles of the BL were analyzed with the help of CFD solutions, provided by the DLR Braunschweig [15]. As a result, the local flow angle was estimated to $\gamma = 10°$. With this knowledge and a given angle of incidence ε the AoA of a VVG can be calculated. Since the usage of the AoA reveals an unknown uncertainty, because of the approximation of the local flow angle γ that changes with both, rudder deflection and yaw angle, the angle of incidence ε will be used throughout this paper.
A template was used to attach the VVGs onto the surface of the VTP. To verify the set angle of incidence a digital angle measuring device was used.

3. MEASUREMENTS TECHNIQUES

A 3-component force balance with SG force transducer was used to measure the side force, the drag and the pitching moment generated by the model. For each measurement point the data acquisition device MGCplus recorded 3000 samples with a sample frequency of 100 Hz. To verify the measured forces, repetition measurements of the exact same configuration were conducted. Based on an uncertainty evaluation and the analysis of the repetition measurements, side force and drag coefficients were measured accurately with a maximal deviation of up to $\Delta\,C_Y = 0.008$ and $\Delta\,C_W = 0.001$. However, no wind tunnel corrections are applied to the measured data.
It might be noted that the VTP is equipped with 150 pressure tabs in six sections distributed over span. However, the conclusion that will be drawn in this paper can be derived without the discussion of the pressure distributions, which will hence not be covered herein.
Oil flow visualization on the entire suction side of the fin and the rudder were conducted to qualitatively investigate the impact of longitudinal vortices on the wall streamlines of the VTP.

4. RESULTS AND DISCUSSION

In this section, the effect of VVGs on the performance of the VTP will be discussed. In preparative wind tunnel runs the parameters of the VVGs have been varied to find the most effective configuration, which will be taken as a reference in the following. This reference configuration is: $n = 5$, $x/c = 58\,\%$, $\Delta\,\eta = 0.095$ and $\varepsilon = 30°$. In section 4.1 the influence of the reference configuration on the flow around the VTP will be introduced.
The second part provides the discussion of the results generated during the VVG parameter study, which covers the variation of the:

1) Spanwise extension
2) Angle of incidence
3) Shape
4) Size and aspect ratio
5) Spanwise separation
6) Chordwise position

As pointed out before, the objective of the second part is to find the sensitivities of the control effect for the different VVG-parameter.

4.1. Effect of VVG

FIG 5 shows the side force coefficient plotted over the yaw angle for the most effective configuration with a rudder

deflection of $\delta = 15°$. For comparison reasons, the $C_Y(\beta)$-curve of the reference measurement without VVG is added.

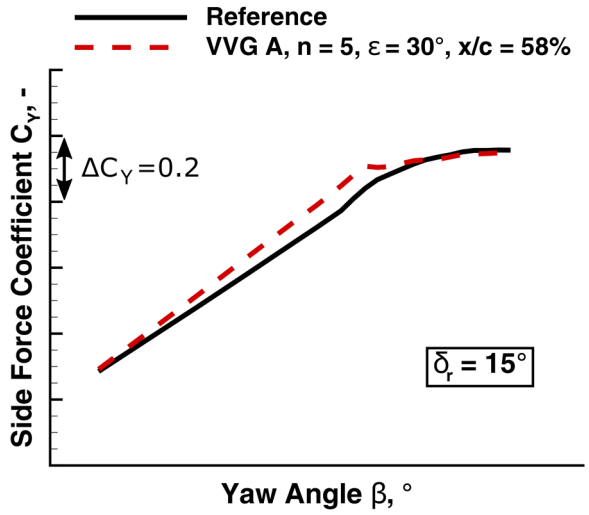

FIG 5: $C_Y(\beta)$-curves of the most effective VVG-config. and reference

At small yaw angles, the configuration with VVGs does not show any gain in side force, but with increasing yaw angle a notable gain is observed. It must be mentioned that at small yaw angles, the flow on the rudder without VVGs is still attached, whereas at larger yaw angles flow separation begins. Hence, if the flow is already attached to the rudder, the VVGs are not beneficial, as one would generally expect. Instead, for $\beta = 0°$ the drag coefficient increases relatively to the reference measurement by $\Delta C_W = 3.4$ %. It is noted that all VVG-configurations showed an increased drag coefficient for the same yaw angle, whereas the comparison at the same side force coefficient showed that drag can be decreased by approximately 28 % in the region of yaw angles, in which separation is prevented (cf. FIG 6).

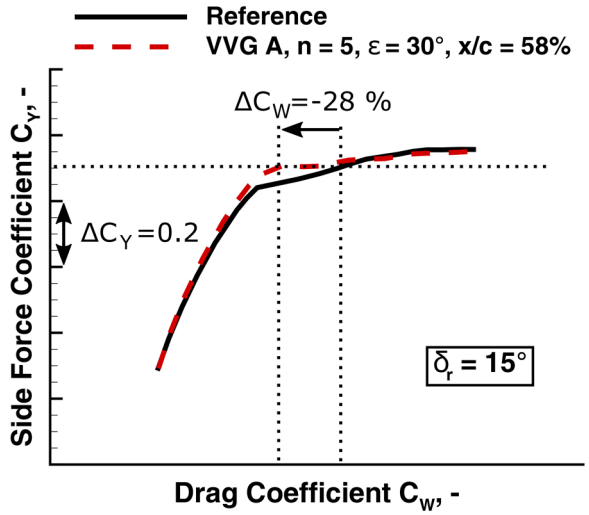

FIG 6: L/D-curves of the most effective-config. and reference

In the case of large rudder deflections, $\delta = 30°$ and $\delta = 35°$, the flow on the rudder is completely detached for the whole range of yaw angles. Here again, the VVG-configurations with $\delta = 30°$ and $\delta = 35°$ show in FIG 7 and FIG 8 an increase of the side force relative to the reference measurement. Furthermore, it appears that the VVG $C_Y(\beta)$-curve is shifted parallel to higher values until the maximal side force coefficient is reached.

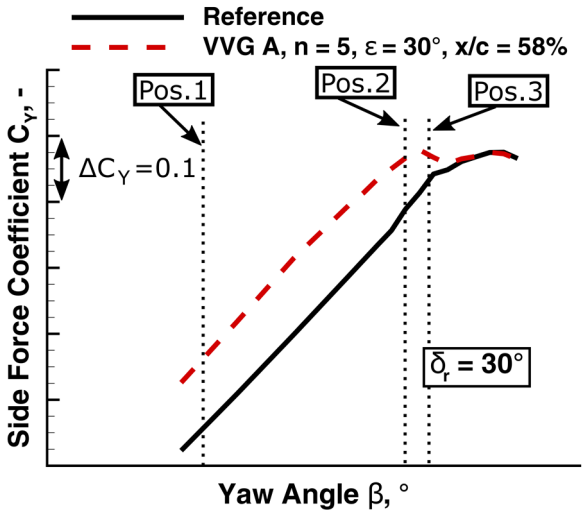

FIG 7: $C_Y(\beta)$-curves of the most effective VVG-config. and reference

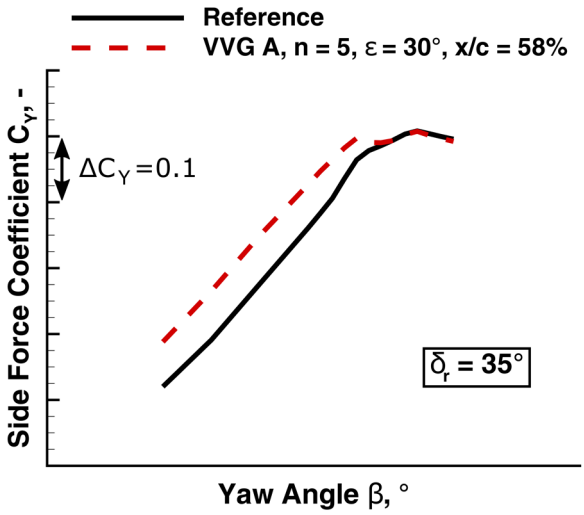

FIG 8: $C_Y(\beta)$-curves of the most effective VVG-config. and reference

It seems that the flow separation is delayed on the rudder due to the longitudinal vortices generated by VVG. Hence, side force coefficient is increased. FIG 9, FIG 10 and FIG 11 show oil flow visualizations for the most effective configuration with $\delta = 30°$ for three different yaw angles: β-Position 1, β-Position 2 and β-Position 3. An overview of the selected sections of the $C_Y(\beta)$-curve is given in FIG 7. The first position represents the flow at a small yaw angle, the second position is close to $C_{Y,max}$ and the third position

is shortly after $C_{Y,max}$. The footprints of the longitudinal vortices, as shown in FIG 9, are clearly visible on the rudder's surface. The vortices generate separation lines (SLs) in the wake of the VVGs, which deflect to the VTP's tip with decreasing distance to the rudder's trailing edge (TE). The deflection of the SLs indicates that the longitudinal vortices tend to move upward due to the three-dimensional flow characteristics of swept wings. Between the SLs, the flow appears to be attached to the rudder. The pressure distributions of the profile sections near the VVG positions confirm this. The upper part of the rudder, where no VVGs are mounted, show a separated flow with a SL at the rudder knee.
These findings support the conclusion that the flow can remain partly attached to the rudder due to the usage of VVGs. However, the visualizations reveal that the area of attached flow is limited to the region directly downstream of the VVGs.
Oil flow visualization at β-Pos. 2 (cf. FIG 10) indicate flow separation at the VTPs tip, which is typical for tapered wings. Regarding the VVG, the SLs are bent towards the tip earlier without even reaching the TE of the rudder. Also, for the uppermost VVGs, the length of the SLs reduces. Hence, longitudinal vortices are deflected earlier when located closer to the tip. Oil flow visualization at a higher yaw angles, as presented in FIG 11, show the SL in the wake of VVG No. 5 disappearing completely. A possible explanation is seen in the interaction with the VTP's tip separation. This grows with increasing yaw angle in the direction of the VTP's root and starts to interact with the longitudinal vortices. Due to this behavior, the effectiveness of VVGs is constant for most of the $C_Y(\beta)$-curve, but decreases at high yaw angles due to separations on the fin. This finding coincides with the $C_Y(\beta)$-curves of FIG 7 and FIG 8. At very high yaw angles, the values for the side force coefficient for all three VVG-configurations fall back on the values of the reference curve. Hence, the effectiveness of VVGs appear sensitive to adjacent separations and therefore has its limitation at very high yaw angles.

The VVG-configuration with $\delta = 35°$ shows the highest measured absolute side force coefficient. In contrast, the VVG-configuration with $\delta = 30°$ shows the largest increase of the side force relative to the reference values. The effectiveness of VVGs seems not only to be dependent on the yaw angle, but also on the deflection of the rudder.
The yaw angle that generates the maximal side force is reduced significantly by VVGs. As a consequent, the drag at maximum side force is also significantly smaller and an increase of the lift to drag ratio of about $L/D \approx 30$ % at $C_{Y,max}$ for $\delta = 30°$ is obtained.

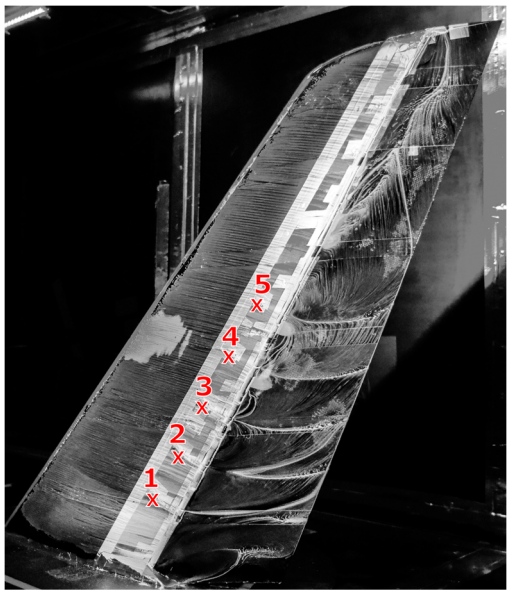

FIG 9: Oil flow visualization for the most effective configuration at β-Position 1

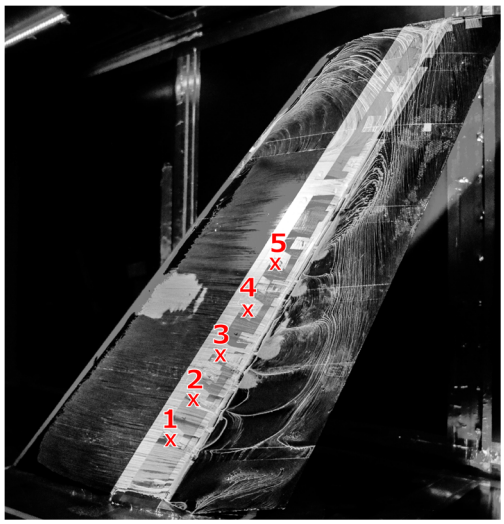

FIG 10: Oil flow visualization for the most effective configuration at β-Position 2

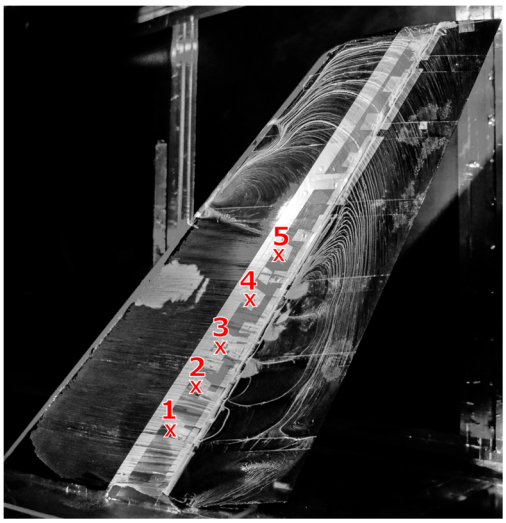

FIG 11: Oil flow visualization for the most effective configuration at β-Position 3

4.2. Parameter Sensitivity Study

Since the present study was conducted with a scaled model in a wind tunnel of limited size, some differences of the flowfield can be expected, e.g. compared to a full-scale VTP. It is therefore interesting to study the sensitivities of various VVG-parameters, to learn which parameter has little influence on the effect and thus could be considered as "robust", and which parameter is very sensitive and should be set with care.
The sensitivity of seven different parameters, namely spanwise extension, angle of incidence, shape, size, aspect ratio, spanwise separation and chordwise position has been studied, each for three different rudder deflections of 15°, 30° and 35°.
However, the comparison of the same parameter configuration at different rudder settings showed that the sensitivities of the parameters is independent from the rudder deflection. Hence, only the results for $\delta = 30°$ will be presented in the following sections.

4.2.1. Spanwise Extension

This variation shows the effect of a spanwise extension of the VVGs. Two configurations with a different number of VVGs, $n = 5$ and $n = 7$, were set at the constant chord length of $x/c = 58$ % and equal spacing of $\Delta\eta = 0.095$. The reduction of the amount from $n = 7$ and $n = 5$ was done by removing the topmost two VVGs close to the VTP tip. The angle of incidence was set to $\varepsilon = 30°$ and the VVG of type A were chosen.
With regard to the parameter study, the comparison between the configurations with 5 and 7 VVGs shows in FIG 12 no significant differences in the side force coefficient. This leads to the conclusion that the upmost two VVGs No. 6 and 7 do not contribute to the gain in the total side force of the VTP. Hence, VVGs appear more effective in the lower part of the VTP.

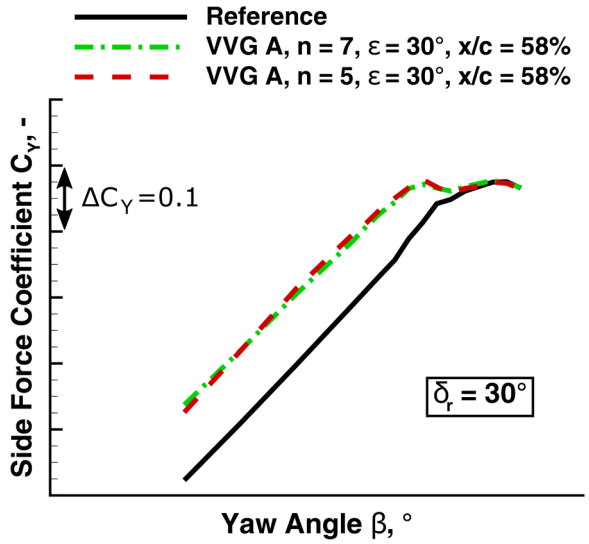

FIG 12: $C_Y(\beta)$-curve: VVG spanwise extension

4.2.2. Angle of Incidence

VVGs are well known to be sensitive to the angle of attack. As discussed in section 2.3 the AoA is closely linked to the angle of incidence ε, where $\varepsilon = 30°$ generates the best effect. To receive notable differences, the angle was changed with $\Delta\varepsilon = 10°$. Hence, the first configuration shows a decreased angle of incidence of $\varepsilon = 20°$ ($\alpha \approx 10°$) and the second configuration an increased value of $\varepsilon = 40°$ ($\alpha \approx 30°$).
FIG 13 shows the $C_Y(\beta)$-curve for the configurations with $\varepsilon = 30°$, $\varepsilon = 20°$ and $\varepsilon = 40°$ accompanied by the curve of the reference measurement. In comparison, the configuration with $\varepsilon = 40°$ indicates a smaller loss in side force coefficient than the configuration with $\varepsilon = 20°$. It should be noted that in the oil flow visualization for the configuration with $\varepsilon = 20°$ no SLs on the rudder in the wake of the VVG are visible, although, at a closer look, footprints of longitudinal vortices are visible directly behind the VVG. This leads to the conclusion that the small ε cannot generate a longitudinal vortex strong enough to remain the flow attached to the rudder. On other hand, the longitudinal vortices decrease the pressure at the rudder knee so that with respect to the reference measurement the side force coefficients are still increased.
It can be concluded that the optimum angle of incidence is somewhere close to $\varepsilon = 30°$, probably a little bit larger. These findings coincide with the in [14] stated optimal range of $18° < \alpha < 23$. As based on the results, and as expected, the angle of incidence ε is a relative sensitive parameter.

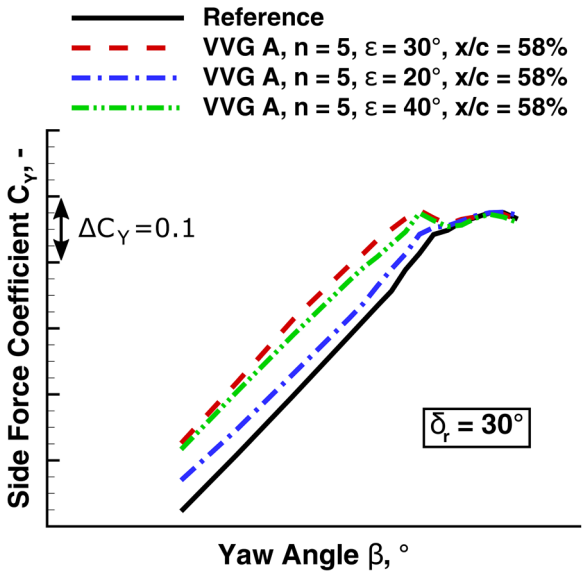

FIG 13: $C_Y(\beta)$-curve: Angle of incidence

4.2.3. Shape

The variation of the shape compares a VVG of type A, which has a square shaped geometry, and a VVG of type B, which has a triangular shaped geometry (cf. FIG 2). The triangular shaped VVG can be understood as a half-model of a delta wing that is capable of reaching greater lift coefficients at high AoA due to its leading-edge vortex. It was assumed that this would enhance the generation of the longitudinal vortex and thus increase the effectiveness of the VVG. To conduct this variation, $n = 5$ VVGs were positioned at $x/c = 58$ % and $\Delta\eta = 0.095$ for both configurations. FIG 14 shows that the configuration with VVGs of type B does not reach the values as it was measured for the configuration with VVGs of type A. Hence,

the angle of incidence of the VVGs of type B was increased to $\varepsilon = 40°$ considering that the benefits are expected to be at greater AoA. As a result, higher side force coefficients were reached. For small yaw angles VVGs of type B with $\varepsilon = 40°$ reach similar side force coefficients as the configuration with VVGs of type A at $\varepsilon = 30°$. It seems that the benefits of a triangular VVGs can be seen at high angles of incidence and at small yaw angles. However, the effectiveness reduces rapidly with increasing yaw angle.
The overall results do not match the expectation, in which triangular VVGs were stated as the more effective shape (cf. [7]). Eventually, further increase of the angle of incidence could increase their effectiveness at large yaw angles, but herein we have found no benefit of triangular over rectangular ones.

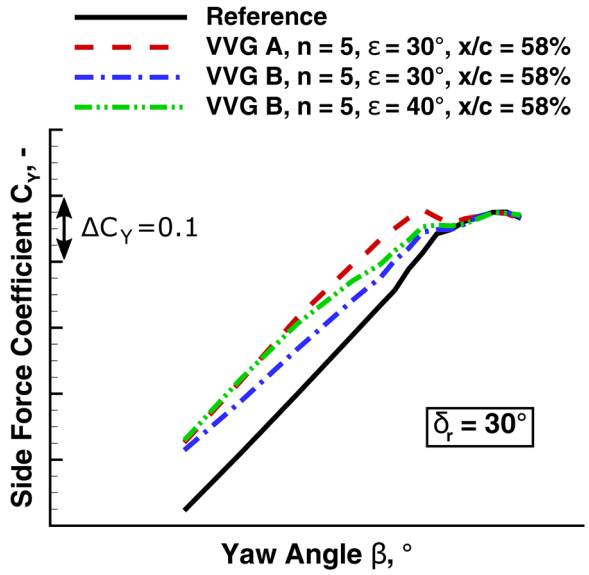

FIG 14: $C_Y(\beta)$-curve: Variation of the shape

4.2.4. Size and aspect ratio

For this investigation the VVG of type A was used as a basis, from which the aspect ratio λ_{VVG} (cf. VVG type C) and the size (cf. VVG type D) were changed. According to the previous parameter studies, the VVGs were mounted at $x/c = 58$ %, with $\Delta\eta = 0.095$ and $\varepsilon = 30°$. The objective of increasing the size of an VVG is to investigate the influence of a stronger longitudinal vortex, which is expected to have a larger vortex diameter and an increased distance of the vortex center to the VTPs surface. The variation of the aspect ratio was conducted to test its dependency on the vortex generation itself. The results are shown in FIG 15.
In the case of the variation of the size, smaller side force coefficients are reached for VVGs of type D. Hence the increase of the longitudinal vortex size does not increase the side force coefficient. Instead, it is slightly decreased, except for the maximum value, where both configurations reach a similar value. At this point it must be noted that the VVG-configuration of type A already generates longitudinal vortices that are strong enough to maintain an attached flow on the rudder (cf. FIG 9). Considering that an attached flow is the main contributor to the increase of the side force, the gain resulted by a bigger vortex is expected to be similar. In fact, the results show that it is less. An explanation could be the increased distance of the vortex center to the surface, in which case the longitudinal vortex is not able to mix the boundary layer sufficiently. Oil flow visualization reveal that for the VVGs No. 4 and 5 SLs are absent at the same yaw angle as it is shown in FIG 10. Furthermore, in comparison to FIG 10 the SLs of the VVGs No. 1, 2 and 3 reach the rudder trailing edge. It appears that due to the usage of larger VVGs at the upper part of the VTP the longitudinal vortices are without any effect and at the lower part the effectiveness is enhanced. Both upper and lower areas combined could explain the deficit in side force coefficient.
However, it must be mentioned that the height of the VVGs were not scaled with respect to the boundary layer thickness as it was recommended in [14]. This leads to the assumption that the lower VVGs must now have reached a beneficial height ratio close to $h/\delta \approx 1$ and the upper VVGs a less effective ratio of $h/\delta > 1$. The BL thickness was estimated to be around $\delta_{root} = 10$ mm at the root and decreases gradually towards the VTP's tip to $\delta_{tip} = 6$ mm. Considering the VVG height of $h = 10$ mm, this result supports the assumption, in which the effectiveness of VVGs depends on the height to thickness ratio h/δ.
In case of the variation of the aspect ratio, the aspect ratio of $\lambda_{VVG} = 2.0$ (VVG type A) was decreased to $\lambda_{VVG} = 1.2$ (VVG type C). With regard to [7], the aspect ratio of the VVG type C was selected too small. The results in FIG 15 confirm this. Still, a slight increase of the side force coefficient relatively to the reference is measured. Further analysis of the Oil flow visualization at β-Pos. 2 reveal that there are no SLs on the ruder. At a closer look, the signs of the existence of longitudinal vortices at the lower part of the rudder are barely visible. However, the reduction of the aspect ratio appears to generate weak longitudinal vortices that have only little effect on the rudder's BL.
Within the investigated parameter range, it can be concluded that the side force coefficient increases with larger aspect ratio and a height to thickness ratio of $h/\delta \approx 1$.

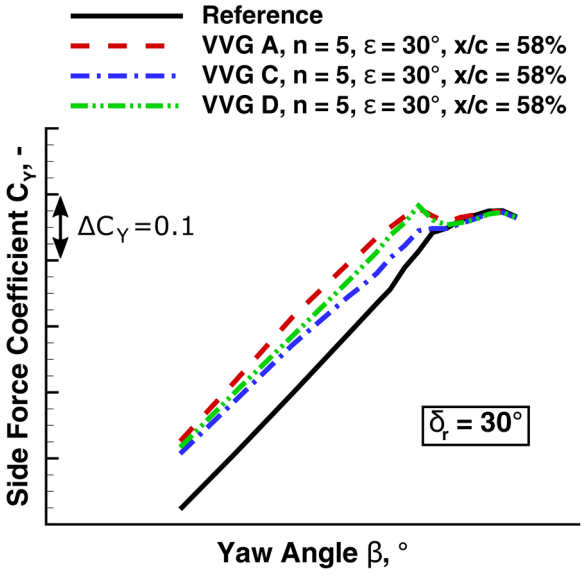

FIG 15: $C_Y(\beta)$-curve: Size and aspect ratio of the VVG

4.2.5. Spanwise separation

The spanwise separation was conducted by taking the configuration with n = 5 VVGs and placing additional VVGs in between, so that the spanwise distance is halved from

$\Delta\eta = 0.095$ to $\Delta\eta = 0.0475$ (cf. FIG 3). The objective of this measure is to investigate the sensitivity of the distance between two VVGs. Possible beneficial interaction between the longitudinal vortices were expected.
As a matter of fact, no significant differences between both configurations are visible in FIG 16. Hence, the halving of the spanwise distance has neither beneficial nor unfavorable effect on the side force coefficient. Conversely, this means that less VVGs with greater spanwise separation are equal effective. A further investigation with larger spanwise separation and a reduced number of VVGs seems desirable.

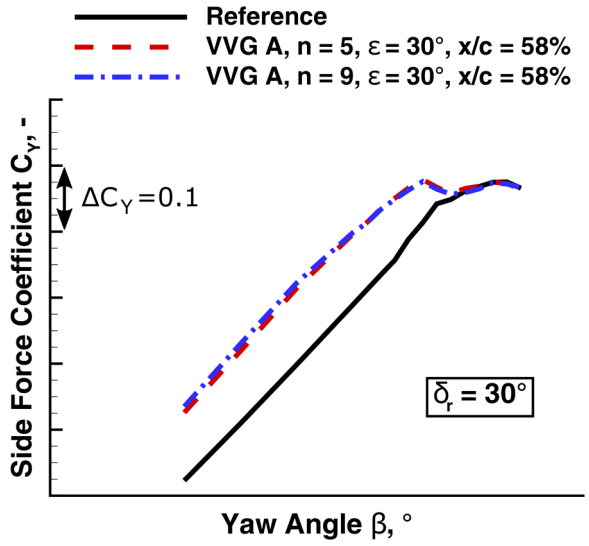

FIG 16: $C_Y(\beta)$-curve: Spanwise separation

4.2.6. Chordwise position

The last investigation deals with the influence of the VVG chordwise position on the rudder flow. For that reason, $n = 5$ VVGs with $\varepsilon = 30°$ and $\Delta\eta = 0.095$ were moved from $x/c = 58$ % to $x/c = 40$ % (cf. FIG 3). It is noted that the local flow angle γ changes due the chordwise shift of the VVGs and thus the angle of incidence needs to be adjusted. Since the shift was realized in the direction to the VTPs LE, where the local flow angle tends to decrease, an increase of the AoA of the VVG is expected. According to the findings of the parameter study of the angel of incidence, slightly larger AoA are not detrimental to the effectiveness. Hence, the angle of incidence was not adjusted. The objective of the investigation was to determine if a greater distance to the SL at the rudder knee is beneficial in terms of the side force coefficient. FIG 17 shows for small yaw angles minor differences in the side force coefficient, but with increasing yaw angle the $C_Y(\beta)$-curve of the configuration with $x/c = 40$ % decreases strongly. The oil flow visualization at β - Pos. 2 shows clearly footprints of longitudinal vortices on the fin in the region directly downstream of each VVG. However, no SLs on the rudder haven been observed. Hence, with increasing distance to the SL at the rudder knee the effectiveness of VVGs reduces. Conversely, these findings suggest that the VVGs would be more effective when positioned closer to the rudder knee.

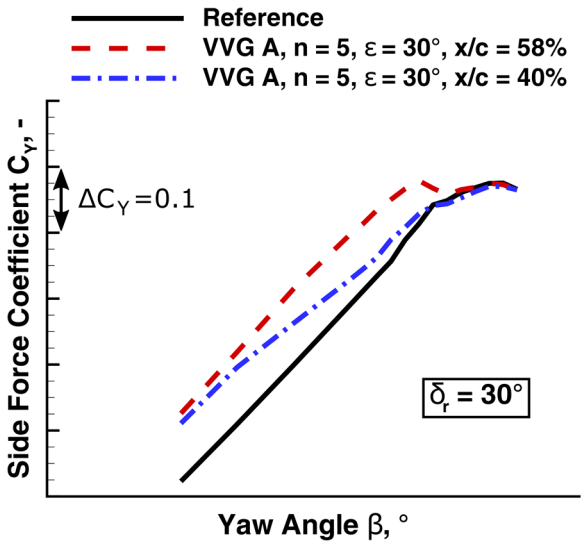

FIG 17: $C_Y(\beta)$-curve: Chordwise position

4.3. Effects of Yaw and Deflection Angle

FIG 18 summarizes the results of the parameter study, in which the percentage increase with respect to the reference measurement over the yaw angle for different rudder deflections is shown.

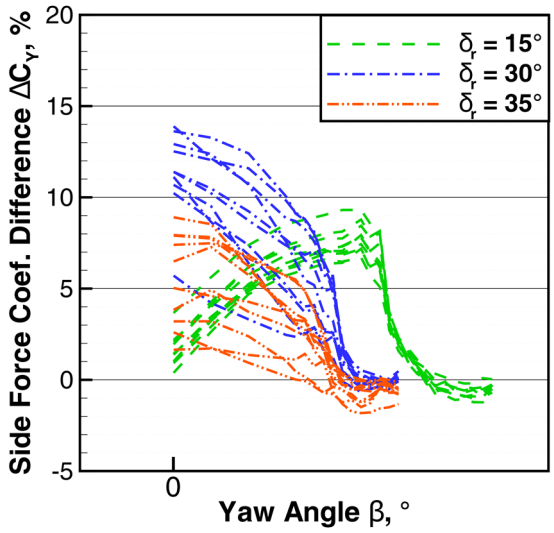

FIG 18: C_Y gain for all configurations of the parameter study

It becomes apparent that the largest increase of about 14 % of the side force coefficient is found at the rudder deflection of $\delta_r = 30°$ at $\beta = 0°$. With increasing yaw angle, the side force gain decreases strongly to zero. Similar behavior is seen for $\delta_r = 35°$, in which the largest gain in side force coefficient is about 9 %, though. The curves for the rudder deflection of $\delta_r = 15°$ show an initial increase of the side force until its maximum with a subsequent drop.
These results show that the effect of the VVGs is in general dependent on the rudder deflection. However, the different parameter settings of the VVGs are not sensitive to the

rudder angle. That means, that a VVG-configuration, which is effective for a certain rudder deflection, is similar effective for other rudder deflections.

5. SUMMARY

The parameter study shows the ability of longitudinal vortices generated by VVGs to maintain the flow attached to the rudder if correct parameters are applied. As a result, the side force of the VTP is increased. Also, results indicate that the reattachment of the rudder's flow is the main contributor to the increase of the side force.
In the direction of greater yaw angle, the gain in side force coefficient is gradually decreasing, because the longitudinal vortices are bend earlier towards the tip without reaching the rudders TE. At very high yaw angles, VVGs appear ineffective, because of separation on the upper part of the fin, which strongly influences the path of the longitudinal vortices. In fact, for the VVGs on the upper part of the VTP longitudinal vortices did not even reach the rudders surface. The maximal side force is limited due to the stalling characteristics of the VTP and consequently could not be enhanced by VVG. However, when VVGs are used the maximal side force is reached at a smaller yaw angle, which leads to a decrease of the total drag and an increase of the lift to drag ratio of about $L/D \approx 30$ %.
Regarding the deflection angle of the rudder, it was observed that the gain in side force coefficient increases with larger deflection angles until $\delta_r = 30°$, in which case an increase of the side force coefficient of up to 14 % is reached. Further deflection to very high angles at $\delta_r = 35°$, reduces the side force coefficient increase.
With respect to the parameter study, results show that some parameters are more sensitive, whereas other parameter, such as the spanwise extension and separation, do not show any reaction to a parameter change. The following summarizes the key conclusions of each investigated parameter:

1) The investigation of the spanwise extension of VVGs revealed that the upmost VVGs tend to be ineffective, which leads to the idea that a further reduction may enhance the efficiency.
2) The increase of the AoA of VVGs is less destructive to the gain in side force coefficient than a decrease.
3) The Variation of the shape showed that triangular shaped VVGs work better at very high AoA, but cannot hold the gain in side force coefficient to higher yaw angles as the rectangular VVGs.
4) Regarding the size of VVGs, it appears that the VVG height to BL thickness ratio of $h/\delta \approx 1$ generates the most effective longitudinal vortices. In terms of the aspect ratio, results confirm that the aspect ratio should not be smaller than two.
5) The positioning of the more longitudinal vortices closer together did not show any substantial enhancement. Anyhow, further results suggest that a reduction of VVG may enhance the efficiency.
6) The results of the Variation of the chordwise positioning suggest mounting the VVGs closer to the rudder knee, where the SL is found for the reference case.

The knowledge gathered from this parameter sensitivity study shows a brief overview of important parameters and could serve as a basis for more detailed investigation or technical implementation on swept and tapered wings.

ACKNOWLEDGEMENTS

This work is part of the collaborative research project AsSaM (Autoritätssteigerung von Steuerflächen durch aktive Maßnahmen) and funded through the Bundesministerium für Wirtschaft und Energie, which is gratefully acknowledged.

REFERENCES

[1] European Aviation Safety Agency, *Certification Specifications and Acceptable Means of Compliance for Large Aeroplanes* CS-25, 2016.
[2] Braukus, M., Foley, *J. M., NASA, Boeing Finish Tests of 757 Vertical Tail with Advanced Technology*, Nov. 2013, URL: https://www.nasa.gov/content/nasa-boeing-finish-tests-of-757-vertical-tail-with-advanced-technology (date of access: 26.03.2017)
[3] Barnstorff, K., *NASA Tests Green Aviation Technology on Boeing ecoDemonstrator*, April 2015, https://www.nasa.gov/aero/nasa-tests-green-aviation-technology-onboeing-ecodemonstrator.html (date of access: 26.03.2017).
[4] Lin, J. C., *Review of research on low-profile vortex generators to control boundary-layer separation*, In: Progress in Aerospace Sciences, 38(4): p. 389–420, 2002.
[5] Rao, D. M., Kariya, T. T., *Boundary-Layer Submerged Vortex Generators for Seperation Control – An Exploratory Study*, AIAA, ASME, SIAM and APS, National Fluid Dynamics Congress, 1988
[6] Lin, J. C., Howard, F. G., *Turbulent Flow Separation Control Through Passive Techniques*, In: AIAA 2nd Shear Flow Conference, p. 976, 1989.
[7] Godard, G. Stanislas, M., *Control of a decelerating boundary layer. Part 1: Optimization of passive vortex generators*. In: Aerospace Science and Technology, 10.3: p. 181–191, 2006.
[8] Radespiel, R., Burnazzi, M., Casper, M., Scholz, P., *Active flow control for high lift with steady blowing,* In: The Aeronautical Journal, 120: p. 171 – 200, 2016.
[9] Shizawa, T., Eaton, J. K., *Turbulence Measurements for a Longitudinal Vortex Interacting with a Three-Dimensional Turbulent Boundary Layer,* In: AIAA, 30(1), 1992.
[10] Shizawa, T., Eaton, J. K., *Interaction of a Longitudinal Vortex with a Three-Dimensional, Turbulent Boundary Layer,* In: AIAA, 30(5), 1992.
[11] Mahmood, S., Scholz, P., Radespiel, R., *Numerical Design of Leading Edge Flow Control over Swept High-Lift Airfoil,* In: Aerotecnica Missili & Spazio, The Journal of Aerospace Science, Technology and Systems, 91(1-2), 2013.
[12] Meunier, M., Brunet, V., *High-Lift Devices Performance Enhancement Using Mechanical and Air-Jet Vortex Generators,* In: Journal of Aircraft, 45(6), 2008.
[13] Bohannon, K., *Passive Flow Control on Civil Aircraft Flaps using Sub-Boundary Layer Vortex Generators in the AWIATOR Programme,* In: 3rd AIAA Flow Control Conference, p. 31776, 2006.
[14] Broadley, I., Garry, K. P., *Effectiveness of Vortex Generator Position and Orientation on Highly Swept Wings,* In: AIAA 15th Applied Aerodynamics Conference, page S. 2319, 1997.
[15] Gebhardt, A, Simulationsergebnisse - Referenzfall. DLR Braunschweig, unveröffentlicht, 2016.